Science Advances
AAAS

advances.sciencemag.org/cgi/content/full/6/40/eabc6521/DC1

# Supplementary Materials for

## Adaptive optics two-photon endomicroscopy enables deep-brain imaging at synaptic resolution over large volumes

Zhongya Qin, Congping Chen, Sicong He, Ye Wang, Kam Fai Tam, Nancy Y. Ip*, Jianan Y. Qu*

*Corresponding author. Email: boip@ust.hk (N.Y.I.); eequ@ust.hk (J.Y.Q.)

Published 30 September 2020, *Sci. Adv.* **6**, eabc6521 (2020)
DOI: 10.1126/sciadv.abc6521

**The PDF file includes:**



**Other Supplementary Material for this manuscript includes the following:**

(available at advances.sciencemag.org/cgi/content/full/6/40/eabc6521/DC1)

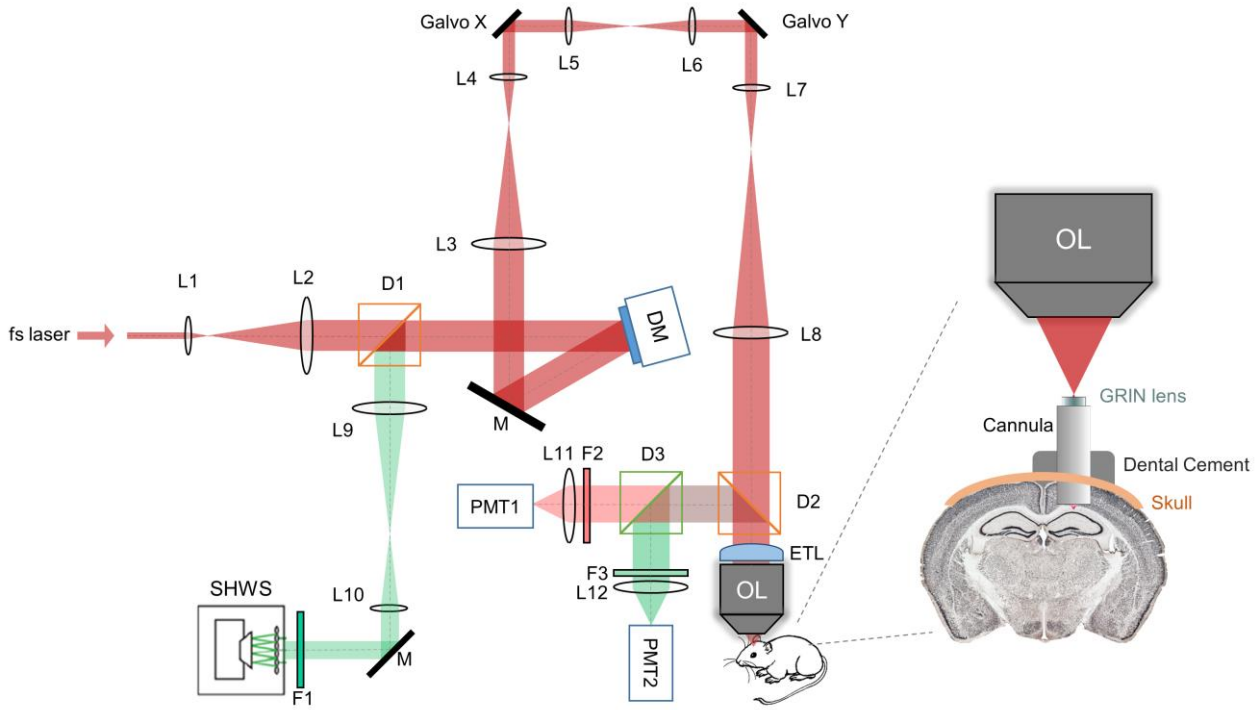


**Figure S1. Schematic diagram of our AO two-photon endomicroscope system for *in vivo* deep brain imaging.** L1-L12: lenses; OL: objective lens; D1-D3: dichroic mirrors; F1-F3: filters; M: mirrors; DM: deformable mirror; SHWS: Shack-Hartmann wavefront sensor; PMT1-2: photomultiplier tubes; ETL: electrically tunable lens.

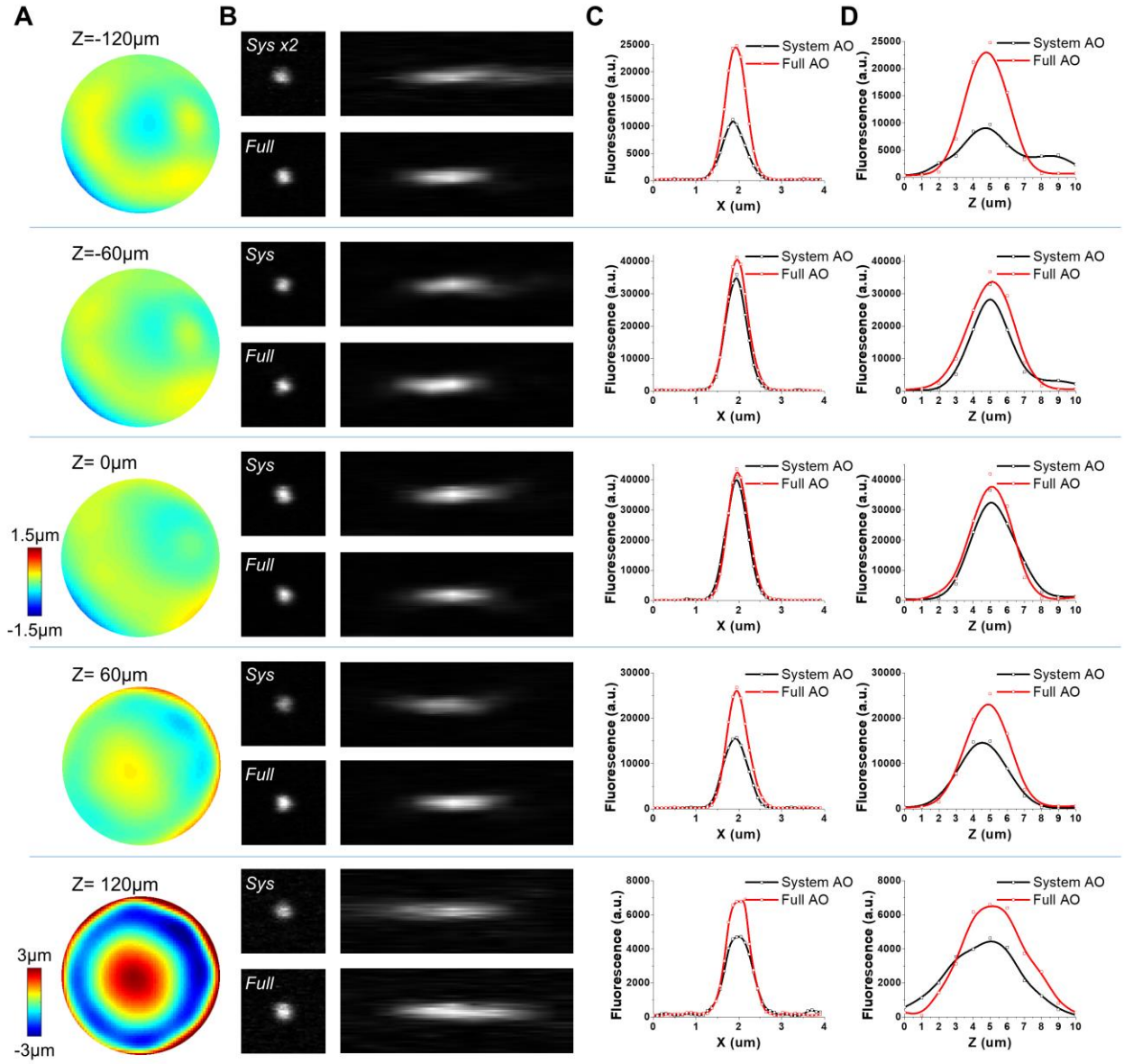


**Figure S2. Characterization of the on-axis aberrations of the GRIN lens.** Column (**A**): The wavefront distortion at different depths along the optical axis. Column (**B**): Lateral and axial PSF measured with fluorescent beads that were 200 nm in diameter at the corresponding depths. Column (**C**): The lateral intensity profile before and after AO correction at the corresponding depths. Column (**D**): The axial intensity profile before and after AO correction at the corresponding depths.

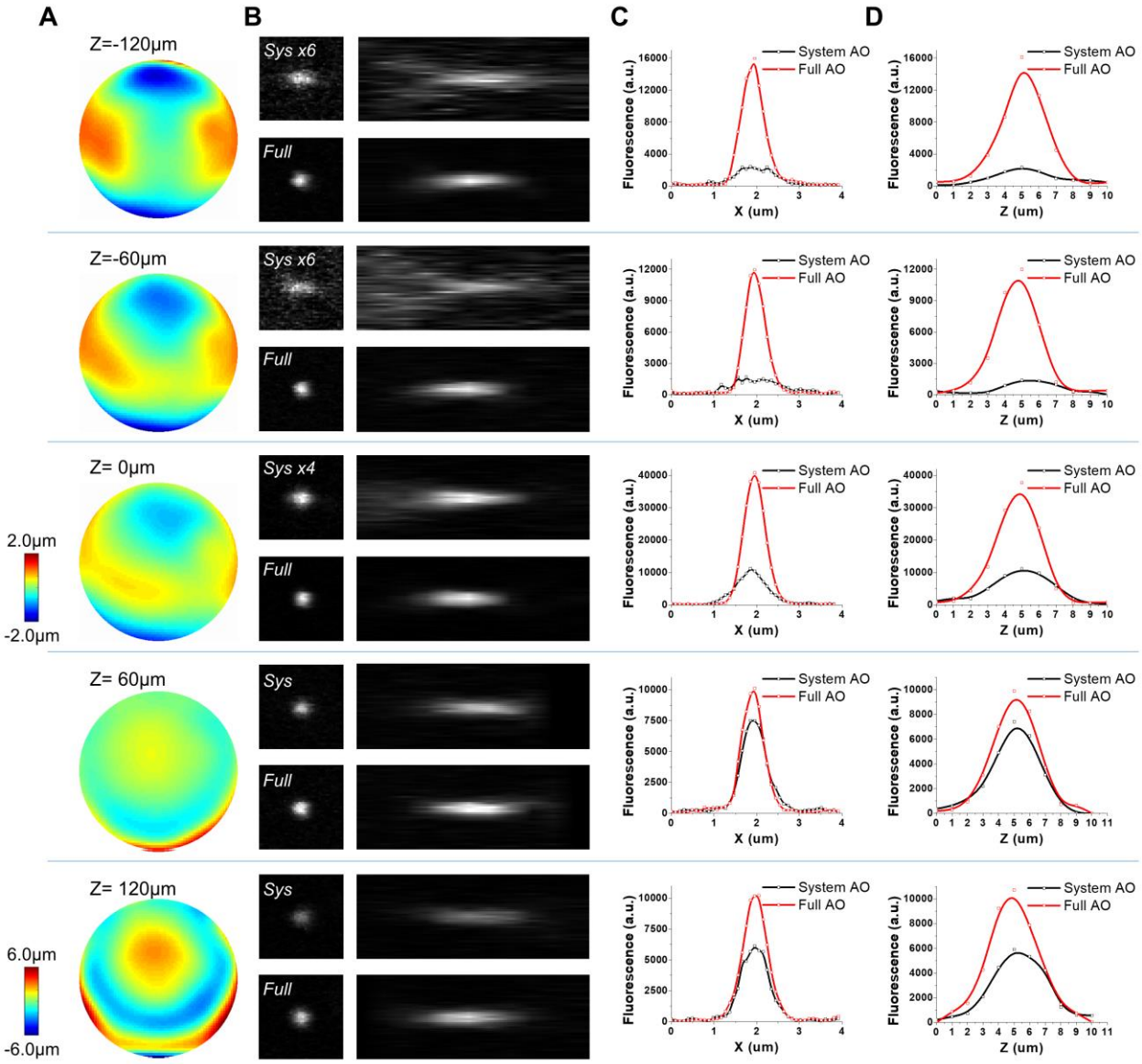


**Figure S3. Characterization of the off-axis (r=60 μm) aberrations of the GRIN lens.** Column (A): (**A**) The wavefront distortion at a distance of 60 μm from the field center at different depths along the optical axis. Column (**B**): Lateral and axial PSF measured with fluorescent beads that were 200 nm in diameter at the corresponding depths. Column (**C**): The lateral intensity profile before and after AO correction at the corresponding depths. Column (**D**): The axial intensity profile before and after AO correction at the corresponding depths.

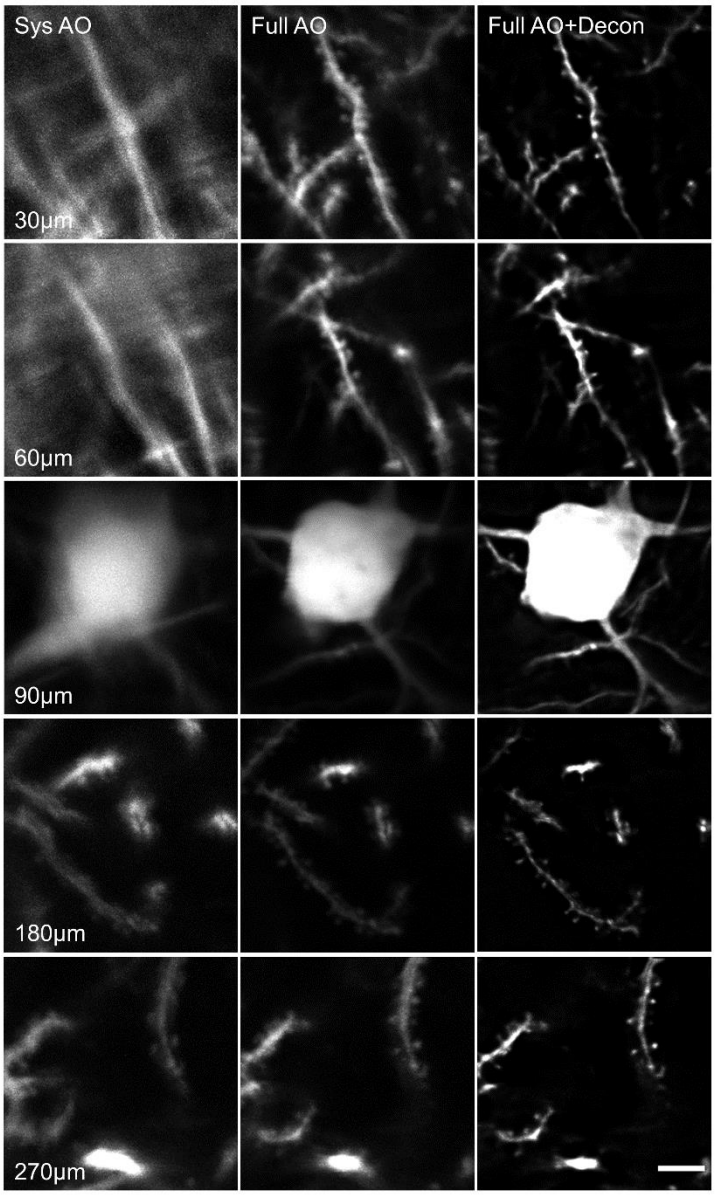


**Figure S4. Comparison of system AO, full AO and full AO with deconvolution at different imaging depths.** The results demonstrate that AO can significantly improve the imaging resolution at all imaging depths. Scale bar: 5 μm.

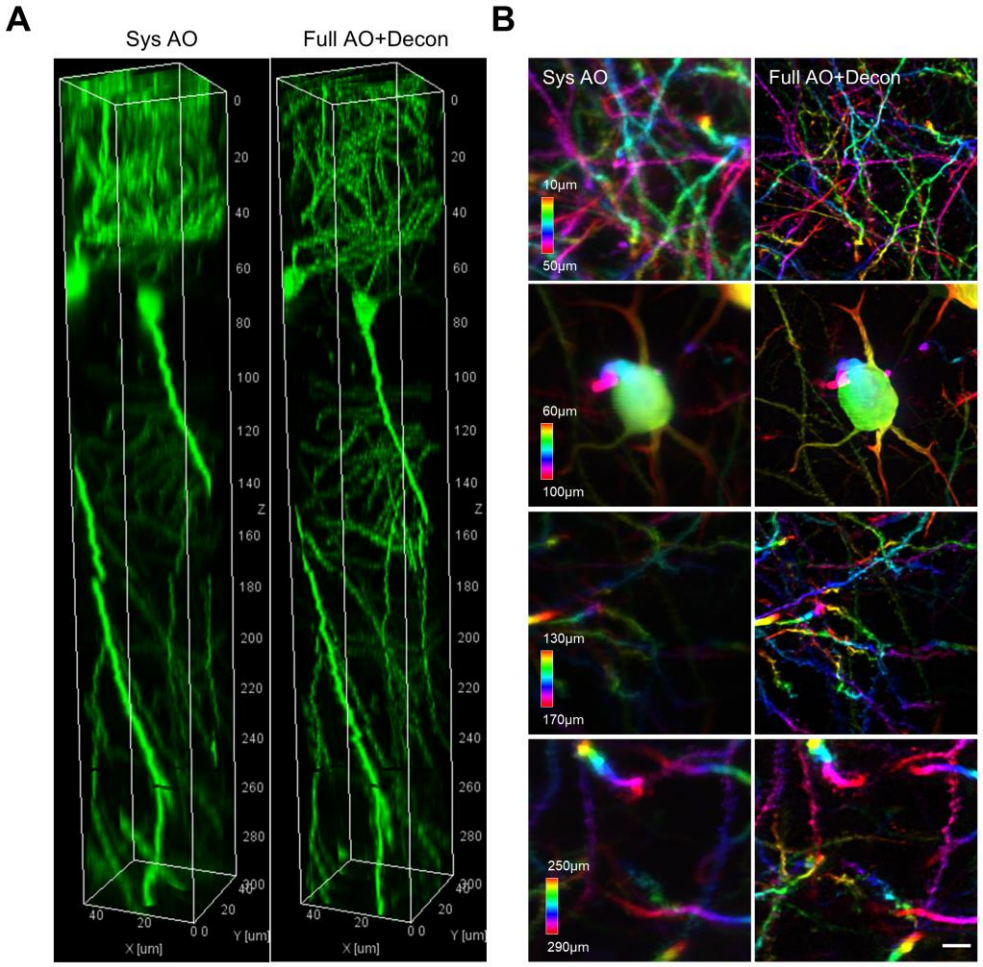


**Figure S5. Three-dimensional imaging of the column located at the center (r=0).** (**A**) In vivo imaging of GFP-labeled CA1 neurons in a 50×50×300 μm$^3$ volume with system (left) and full (right) AO correction. (**B**) MIPs of four subvolumes with system (left) and full (right) AO correction where the structures are color-coded by depth. Scale bar: 5 μm.

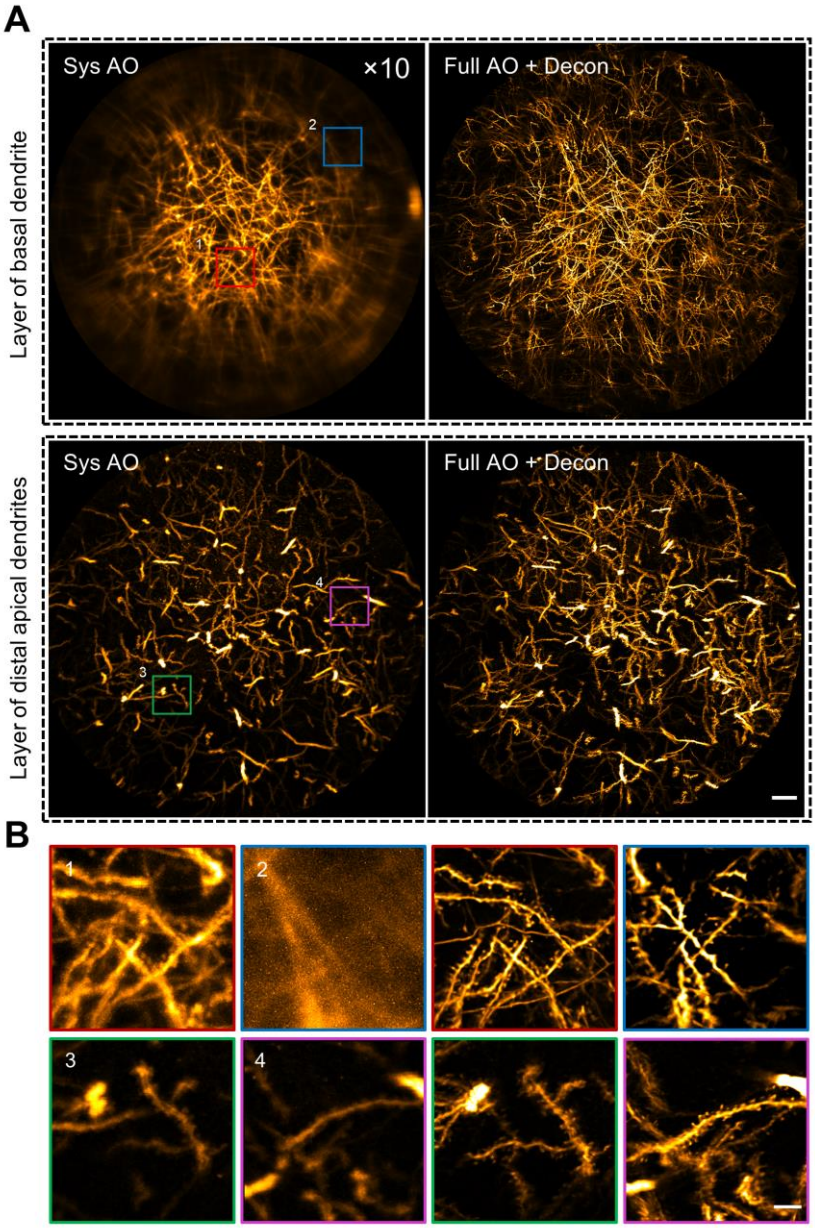


**Figure S6. AO improves resolution over a large FOV.** (**A**) MIPs of the basal dendrite layer and the distal apical dendrite layer with system (left) and full (right) AO correction. The entire FOV is 300 µm in diameter. Scale bar: 20 µm. (**B**) Left: four magnified views of the sub-regions indicated by the numbered boxes in (A). Depth range of projection for the layer of basal dendrites: 20-50 µm; and for layer of distal apical dendrites: 190-220 µm. Scale bar: 5 µm.

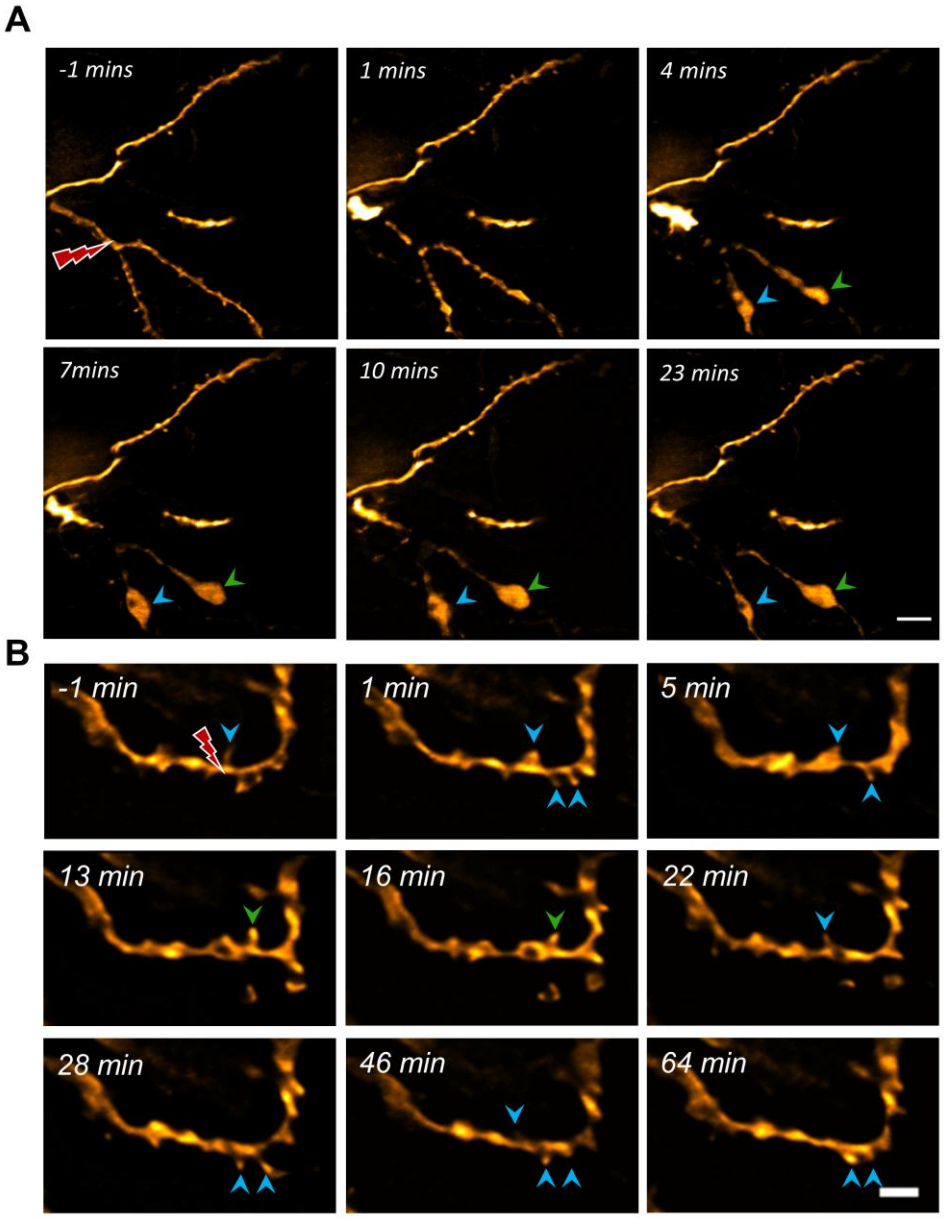


**Figure S7. Time-lapse imaging of dendritic dynamics after laser injury.** (**A**) Laser cutting of dendritic branches leads to rapid and prolonged degeneration that resembles Wallerian axonal degeneration. The bead-like formation at the distal end of the dendrites were indicated by the colored arrowheads. Scale bar: 5 µm (**B**) Laser-mediated micro-lesion of dendritic shaft causes recurrent spinogenesis near the site of injury. The blue and green arrowhead indicate recurrent spine and newly-appeared spine, respectively. Scale bar: 2 µm.

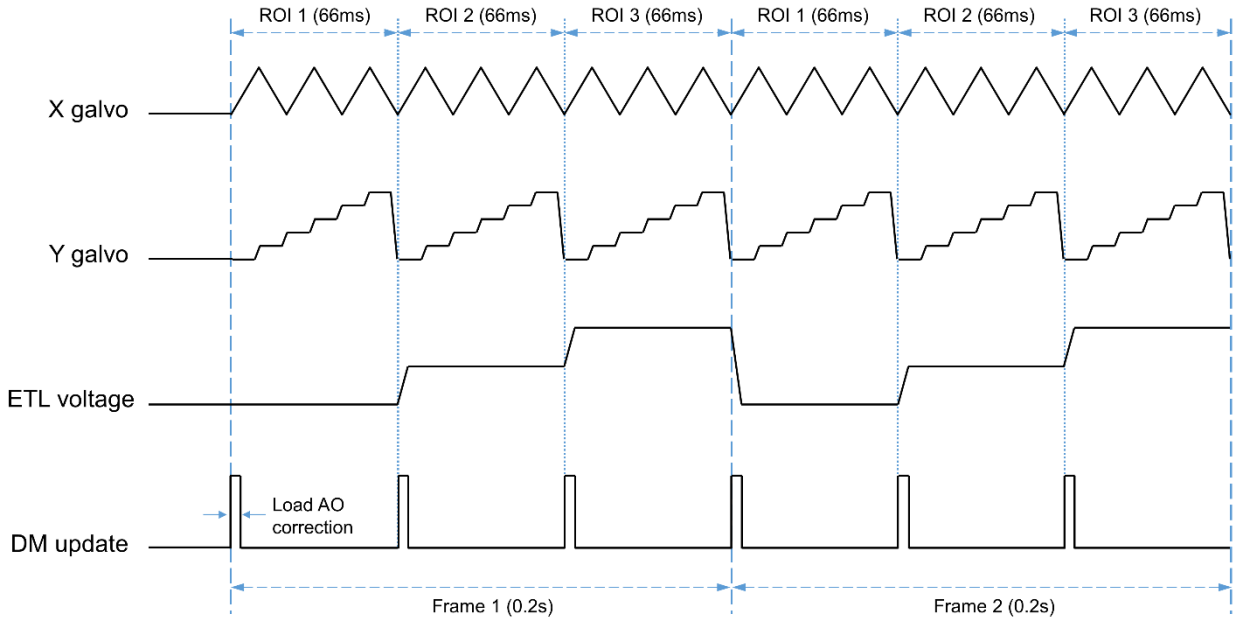


**Figure S8. Control signals of x, y scanners, the ETL and the DM for random-access multiplane imaging.**

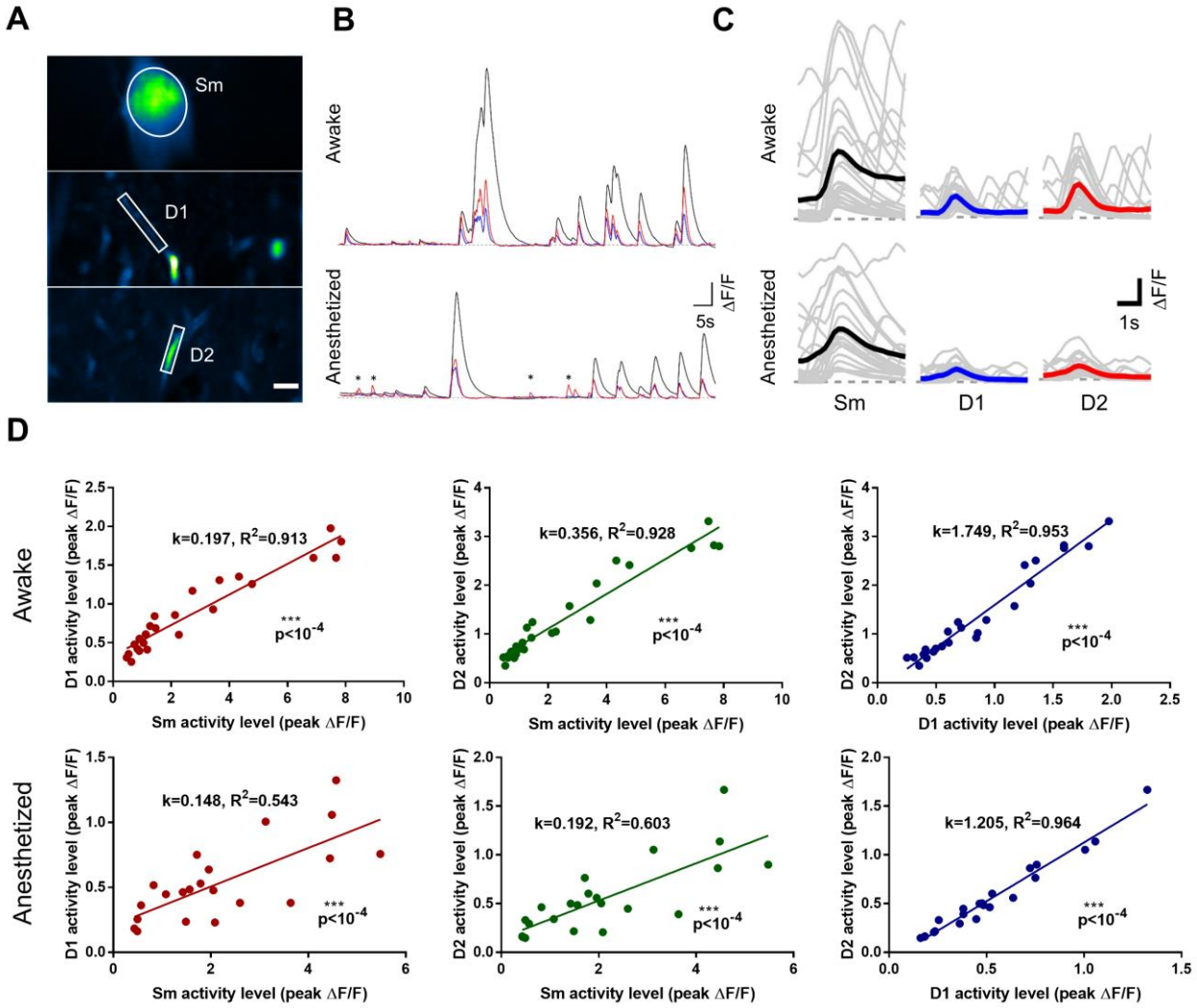


**Figure S9. Correlated somato-dendritic spontaneous activity of hippocampal CA pyramidal neuron is brain-state dependent.** (**A**) *In vivo* multiplane calcium imaging of somato (Sm) and dendritic (D1, D2) activity of single neuron in mice hippocampus. Images are shown as STD projection of the 600 frames. Scale bar: 5μm. (**B**) Calcium transients (ΔF/F) of soma and dendrites shown in (A) under mice wakefulness (upper) and isoflurane-induced anesthesia (lower). Black: Sm, Blue: D1, Red: D2. The asterisks indicate the unpaired dendritic transients appeared in isoflurane anesthesia. (**C**) Firing events of soma (Sm) and dendrites (D1, D2) at different brain states. Grey and colored curves represent the individual and average event, respectively. (**D**) Relationship between activity strength of soma and dendrites under mice wakefulness and anesthesia.

## Table S1. Wavefront sensing and imaging parameters.

| Figure No. | Fluorescence labels | Excitation power(mW) | (r, θ,z) coordinates /(μm, deg, μm) | Subunit volume ($\mu m^3$) | Voxel volume($\mu m^3$) | Pixel rate (pixels/s) | Average frames/slice | Corrective field($\mu m^2$) | Guide star integration(s) |
|---|---|---|---|---|---|---|---|---|---|
| Fig. 1C | Green fluorescence beads /Rhodamine 6G | 30 | (0,0,-90) | 50×50×40 | 0.097×0.097×1 | 256K | No | 30×30 | 1 |
| Fig. 1E | Green fluorescence beads /Rhodamine 6G | 50 | (60,180,-90) | 50×50×40 | 0.097×0.097×1 | 256K | No | 30×30 | 1 |
| Fig. S2B | Green fluorescence beads /Rhodamine 6G | 30 | (0,0,-150~150) | 50×50×40 | 0.097×0.097×1 | 256K | No | 30×30 | 1 |
| Fig. S3B | Green fluorescence beads /Rhodamine 6G | 50 | (60,180,-150~150) | 50×50×40 | 0.097×0.097×1 | 256K | No | 30×30 | 1 |
| Fig. 2A | GFP | 30 | (60, -162, -150~150) | 50×50×40 | 0.097×0.097×1 | 256K | No | 30×30 | 1~2 |
| Fig. S4 | GFP | 50 | (96,106, -150~150) | 50×50×40 | 0.097×0.097×1 | 256K | No | 30×30 | 1~3 |
| Fig. S5A | GFP | 30 | (0,0,-150~150) | 50×50×40 | 0.097×0.097×1 | 256K | No | 30×30 | 1~2 |
| Fig. S7 | GFP | 30 | (0,0,-95--55) | 50×50×40 | 0.097×0.097×1 | 256K | No | 30×30 | 1 |
| Fig. 3A (upper) | GFP | 30 | (0~150,0~360, -90~-50) | 50×50×40 | 0.097×0.097×1 | 984K | 16 | 30×30 | 1 |
| Fig. 3A (lower) | GFP | 30 | (0~150,0~360, -20~20) | 50×50×40 | 0.097×0.097×1 | 128K | No | 30×30 | 1 |
| Fig. S6A (upper) | GFP | 30 | (0~150,0~360, -140~-100) | 50×50×40 | 0.097×0.097×1 | 128K | No | 30×30 | 1 |
| Fig. S6A (lower) | GFP | 30 | (0~150,0~360, 30~70) | 50×50×40 | 0.097×0.097×1 | 256K | No | 30×30 | 1 |
| Fig. 5B | GCaMP6s | 30 | P1: (84, -71, -99)<br>P2: (80, -55, -42)<br>P3: (79,78,-78) | 50×26 (1 slice) | 0.195×0.195 (1 slice) | 507K | No | 30×30 | 1 |
| Fig. 5D | GCaMP6s | 30 | P1: (64, -1.7, -119)<br>P2: (93, -83, -119)<br>P3: (86, 82, -109) | 50×26 (1 slice) | 0.195×0.195 (1 slice) | 507K | No | 30×30 | 1 |
| Fig. 6B | GCaMP6s | 30 | P1: (156, -88, -108)<br>P2: (79, 78, -83)<br>P3: (61, 81, -57) | 50×26 (1 slice) | 0.195×0.195 (1 slice) | 507K | No | 30×30 | 1 |
| Fig. S9A | GCaMP6s | 30 | P1: (156, -88, -108)<br>P2: (80, 78, -80)<br>P3: (64, 81, -53) | 50×26 (1 slice) | 0.195×0.195 (1 slice) | 507K | No | 30×30 | 1 |

**Movie S1. AO enables multiplane $Ca^{2+}$ imaging of pyramidal neuron at synaptic resolution in awake behaving mice.** Three planes (P1-3) were sequentially captured at 5Hz for calcium imaging of neuronal somata, dendrites and spines, respectively, in the hippocampus CA1 during mice wakefulness.

**Movie S2. AO enables accurate recording of calcium transients by eliminating the crosstalk of neighboring neurons.** Three ROIs in the stratum pyramidale of hippocampus CA1 were sequentially captured at 5Hz. With AO full correction, the neighboring neurons can be distinguished from each other without cross talk of the fluorescence signal.

**Movie S3. Simultaneous Ca2+ imaging of somato and dendritic activity of single pyramidal neuron in awake mice.** The soma and two pyramidal dendrites of a pyramidal neuron in hippocampus CA1 were selected for near simultaneous $Ca^{2+}$ imaging. It shows that somato and dendritic activity are highly correlated.